

Chapter 1

Overview

1.1 Introduction

For the next decade, the Fermilab Tevatron Collider remains the high energy frontier of particle physics. The luminosity enhancement provided by the Main Injector dramatically increases the discovery reach and, in conjunction with the upgrade of the collider detectors, moves the experimental program into a regime of *precision* hadron collider physics. Precision capability at the energy frontier will allow simultaneous attack on the open questions of high energy physics from many complementary directions, including:

- characterization of the properties of the top quark
- a global precision electroweak program
- direct search for new phenomena
- tests of perturbative QCD at Next-to-Leading-Order and large Q^2
- constraint of the CKM matrix with high statistics B decays

Each of these topics has the potential for revealing new physics; taken together they offer the most comprehensive discovery potential anywhere in particle physics for at least another decade.

The high luminosity Tevatron of Run II requires extensive changes to the experimental apparatus. We have applied 10 years of experience with CDF and Tevatron physics in the design of an upgraded CDF detector with many powerful new features. This report is a description of the design and expected performance of this upgrade, which we call CDF II.

We devote the rest of Chapter 1 to some history, a tabulation of our design goals, and a brief overview of the upgrade detector and project plan.

In Chapter 2 we motivate the detector design with a quick review of the physics program, extrapolating from our understanding of Run I to the prospects for Run II.

Chapters 3 through 7 describe the motivation and implementation of the CDF II integrated tracking system, and its expected performance for tracking and b-tagging out to $|\eta| = 2$ and in the presence of multiple interactions.

Chapter 8 describes the reuse of the central calorimeter, and Chapter 9 describes the new scintillating tile calorimeter in the plug region.

Chapter 10 describes the improvements to the central muon systems and the addition of muon coverage beyond $|\eta| = 1.0$.

Chapter 11 describes the new pipelined data acquisition system with bandwidth increased by a factor of ten over the old design.

Chapter 12 describes the new deadtimeless trigger system, with tracking at Level-1 and impact parameter discrimination at Level-2.

Chapter 13 describes the off-line computing challenge and Chapter 14 describes the needed facilities support, including the continued use of the superconducting solenoid.

We are confident that this design and a data set increased by a factor of 20 or more will put CDF II and the Tevatron in the exciting position to discover physics beyond the Standard Model.

1.2 History

The Collider Detector at Fermilab (CDF) is a general purpose experiment for the study of $p\bar{p}$ collisions at $\sqrt{s} = 1.8$ TeV at the Fermilab Tevatron Collider. First collisions were produced and detected in October of 1985, and the Tevatron and CDF performance have evolved together to yield data sets of ever in-

creasing sensitivity:

- $\sim 25 \text{ nb}^{-1}$ in 1987
- $\sim 4.5 \text{ pb}^{-1}$ in 1988-1989 (Run 0)
- $\sim 19 \text{ pb}^{-1}$ in 1992-1993 (Run Ia)
- $\sim 90 \text{ pb}^{-1}$ in 1994-1996 (Run Ib)

During the 1988 run the Tevatron met and surpassed its design luminosity of $1 \times 10^{30} \text{ cm}^{-2} \text{s}^{-1}$. The 1994 accumulation utilized instantaneous Tevatron luminosities in excess of $2 \times 10^{31} \text{ cm}^{-2} \text{s}^{-1}$.

The particle physics returns on this steadily evolving sensitivity include the discovery of the top quark and an accurate measurement of its mass $m_t = 176.8 \pm 6.5$, precision measurement of $m_W = 80.41 \pm 0.180 \text{ GeV}/c^2$, measurement of the inclusive jet cross section out to transverse energies of 400 GeV, precision measurement of many b hadron lifetimes, and many of the most stringent limits on non-standard processes. The complete CDF physics archive (see Chapter 15), as of 1 September 1996, is a collection of over 100 published papers ranging over the full state of the art in hadron collider physics.

1.3 Design Parameters

We describe here the relevant conditions of the Tevatron Run II environment, and the physics driven detector performance requirements which we demand there.

1.3.1 Accelerator Configuration

The stated goal of Tevatron Run II is the accumulation of 2 fb^{-1} at $\sqrt{s} = 2.0 \text{ TeV}$, using luminosities up to $2 \times 10^{32} \text{ cm}^{-2} \text{s}^{-1}$. This modest increase in the Tevatron energy has a major impact on physics, (for instance increasing the $t\bar{t}$ yield by 40%) but little impact on the detector performance. Detector issues are driven instead by the luminosity, the number of bunches, and the time between crossings.

The crossing time defines an overall time constant for signal integration, data acquisition and triggering. Two crossing times are discussed for Run II: 396 ns for 36 bunches and 132 ns for 108 bunches. With either of these short times, detectors with long collection times experience pile-up, and trigger and readout latency requires pipelines. Much of the CDF upgrade is necessitated by the new time structure.

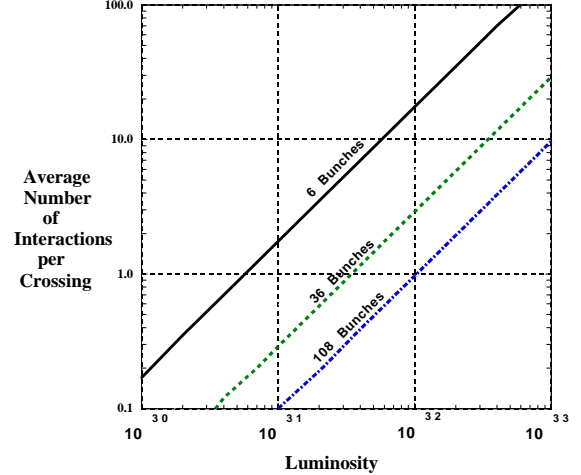


Figure 1.1: \bar{N} for various conditions at CDF. 36 bunches $\equiv 396 \text{ ns}$ crossings, 108 bunches $\equiv 132 \text{ ns}$ crossings

The number of bunches and the luminosity together determine another key design input, \bar{N} , the average number of overlapping interactions in a given beam crossing. \bar{N} is displayed as a function of luminosity and crossing rate in Fig 1.1.

This detector design targets two sets of operating conditions for Run II:

- $\mathcal{L} = 1 \times 10^{32} \text{ cm}^{-2} \text{s}^{-1}$, 396 nsec bunch, $\bar{N} \sim 3$,
- $\mathcal{L} = 2 \times 10^{32} \text{ cm}^{-2} \text{s}^{-1}$, 132 nsec bunch, $\bar{N} \sim 2$

\bar{N} is Poisson-distributed, and a prudent design should be robust on the tails as well as the mean. To fix our upper limit, we recognize the possibility of the hypothetical, but not unreasonable situation

- $\mathcal{L} = 2 \times 10^{32} \text{ cm}^{-2} \text{s}^{-1}$, 396 nsec bunch, $\bar{N} \sim 6$.

When occupancy or pile-up from multiple interactions are important, we will use the conditions $N = 0, 3$, and 6 extra overlapping minimum bias events to evaluate detector performance and margins.

1.3.2 Physics Performance Requirements

A comprehensive summary of the Tevatron Run II physics objectives is presented in Chapter 2. The complexity of the hadronic environment, coupled with the richness and frequent subtlety of the physics signatures, dictates a “general purpose” detection strategy:

- The detector should be able to trigger on and measure as many individual elements of each event as possible.

The ability to compare many independent measurements, across different samples, or even across the same event, leads to a powerful analysis framework where the data itself provides the ultimate precision in the calibration of the hardware and the control of systematic effects. With large data sets at the Tevatron Collider this precision can be applied in a surprising number of different regimes. For example:

- Classic “precision” measurements, such as $\delta m_W \leq 40 \text{ MeV}/c^2$ and $\delta m_t \leq 3 \text{ GeV}/c^2$.
- The baseline survey of the top sector, utilizing secondary vertex based flavor discrimination and precision kinematic reconstruction.
- The search for quark compositeness via the jet E_T spectrum, requiring detailed understanding of calorimeter response.

Many other examples from the physics program outlined in Chapter 2 lead to the following physics performance goals for the CDF II Detector. There are some new capabilities here but all of these goals are reasonable extrapolations based on performance achieved and understood in Run I. We emphasize that these are *goals*.

In either of the two main Run II Tevatron scenarios, CDF II should:

- Reconstruct charged particle tracks with efficiency greater than 95%, over the full range $|\eta| \leq 2.0$.
- Measure charged particle momenta with precision of $\delta p_T/p_T^2 = 0.1\%$ over the range $|\eta| \leq 1.0$, and with precision adequate for lepton identification, $\delta p_T/p_T^2 \sim 0.4\%$, over the range $1.0 \leq |\eta| \leq 2.0$.
- Trigger on, identify, and reconstruct the kinematics and charge of e and μ leptons with high efficiency over the full range $|\eta| \leq 2.0$.
- Tag secondary vertices with the greatest possible efficiency over the full range $|\eta| \leq 2.0$ and over the full interaction region, and trigger on displaced impact parameters over the widest practical range out to $|\eta| = 2.0$.

- Trigger on, identify, and reconstruct the kinematics of photons over the range $|\eta| \leq 2.0$.
- Trigger on and reconstruct jets over the range $|\eta| \leq 3.0$, measure jet energies with resolution of $\sigma_{E_T} = 10\% \cdot E_T + 1 \text{ GeV}$ and with absolute energy scale precision better than 2.5%.
- Measure particle types using dE/dx and time-of-flight in the region $|\eta| \leq 1.0$.

Most (but not all) of these goals will be met in the baseline proposal. See Sec. 1.5 for further detail on this point.

1.4 The CDF II Detector

CDF II is a general purpose solenoidal detector which combines precision charged particle tracking with fast projective calorimetry and fine grained muon detection.

The detector is shown in a solid cutaway view on the cover of this report, and in an elevation view in Fig. 1.2. Tracking systems are contained in a superconducting solenoid, 1.5 m in radius and 4.8 m in length, which generates a 1.4 T magnetic field parallel to the beam axis. The status of the solenoid is discussed in Chapter 14. Calorimetry and muon systems are all outside the solenoid. The main features of the detector systems are summarized below and described in greater detail in Chapters 3 to 12. We use a coordinate system where the polar angle θ is measured from the proton direction, the azimuthal angle ϕ is measured from the Tevatron plane, and the pseudo-rapidity is defined as $\eta = -\ln(\tan(\theta/2))$.

1.4.1 Tracking Systems

Efficient, precision charged particle tracking is at the heart of the CDF analysis technique. An incomplete catalog of some of the applications of charged particle tracking at the Tevatron Collider includes:

- Efficient, precision reconstruction of track momentum for measurements at both high (m_W) and low ($B \rightarrow J/\psi K$) p_T .
- The ability to combine tracks with information from EM calorimetry or muon chambers to provide efficient electron and muon identification with excellent purity at both the trigger and off-line level.

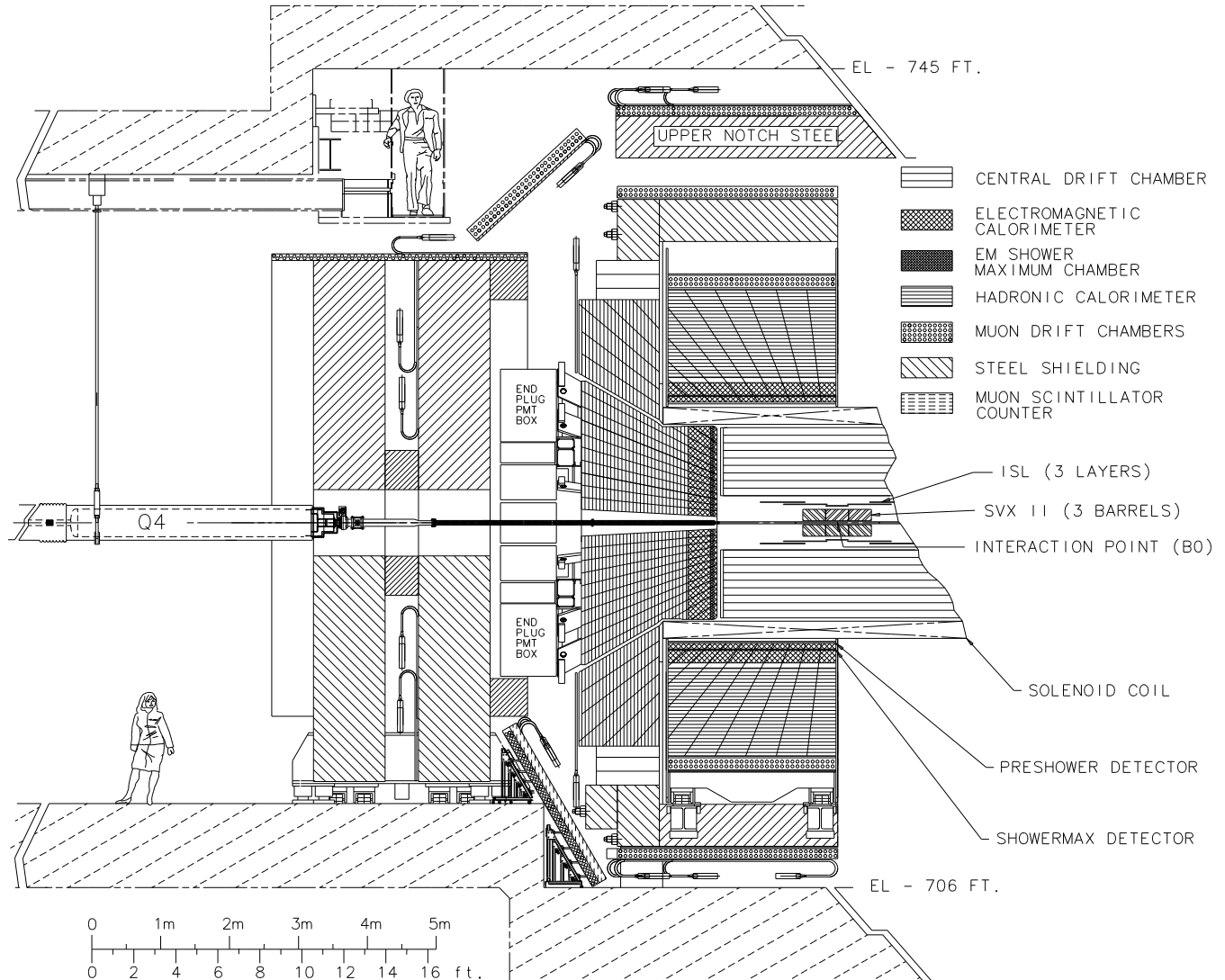


Figure 1.2: Elevation view of one half of the CDF II detector

- Precision reconstruction of track impact parameter and efficient reconstruction of tracks in dense jets, to provide b-tagging which is essential for top physics and searches for new phenomena.
- The ability to rule out tracks in combination with information from EM calorimetry in order to provide efficient photon identification at both the trigger and off-line level.
- The ability to collect low bias triggers on tracks alone.
- The measurement of isolated track momenta as the primary tool and starting point for the calibration of calorimeter response in both the EM and hadronic systems.
- Precision reconstruction of the interaction vertex z coordinate to allow counting and calibration of multiple interactions.
- The ability to map and quantify material in the tracking volume using the distribution of photon conversions.

To meet our physics goals we must maintain or improve the efficiency for these capabilities at high luminosity, and add these capabilities for tracks in the region $1.0 \leq |\eta| \leq 2.0$. At the same time, we wish to remedy the weaknesses of the Run I system, notably the mismatch between the acceptance and capabilities of the central drift chamber and the silicon vertex detector.

For Run II, we propose an optimized “integrated tracking system” shown schematically in Fig. 1.3. At large radii, a new open cell drift chamber, the COT, recovers the functionality of the CTC at high luminosity over the region $|\eta| \leq 1.0$. Inside the COT, a silicon “inner tracker” is built from two components. A micro-vertex detector at very small radii establishes the ultimate impact parameter resolution. Two additional silicon layers at intermediate radii provide p_T resolution and b-tagging in the forward region $1.0 \leq |\eta| \leq 2.0$, and *stand-alone* silicon tracking over the full region $|\eta| \leq 2.0$.

As discussed in Chapter 7, stand-alone silicon segments allow integrated tracking algorithms which maximize tracking performance over the whole region $|\eta| \leq 2.0$. We show there that a good signal to noise ratio for the silicon segments requires at least five measurements. Good efficiency then requires the

addition of a sixth layer everywhere. This will be placed at 20 cm in the region $|\eta| \leq 1.0$ and at 22 cm in the region $1.0 \leq |\eta| \leq 2.0$. In the central region, the stand-alone silicon segment can be linked to the full COT track to give excellent p_T and impact parameter resolution. Beyond $|\eta| = 1.0$, where the COT acceptance and efficiency falls precipitously, a seventh silicon layer at 28 cm is required in order to recover acceptable p_T and impact parameter resolution for a stand-alone silicon track (not segment!) in that region.

The main parameters of the integrated tracking system are summarized in Table 1.1, and the system components are described briefly below, and in greater detail in Chapters 4, 5, and 6. The motivation of the system is described in greater detail in Chapter 3, and its performance is benchmarked in Chapter 7.

1.4.1.1 Central Outer Tracker: COT

Tracking in the region $|\eta| \leq 1.0$ will be done with an open cell drift chamber, the COT, covering radii between 44 and 132 cm. This device replaces the venerable CTC of Run 0 and Run I, which would suffer from severe occupancy problems at $\mathcal{L} \geq 1 \times 10^{32} \text{ cm}^{-2} \text{s}^{-1}$.

The design goal of the COT is to reproduce the functionality of the CTC, but using small drift cells and a fast gas to limit drift times to less than 100 ns. The basic drift cell will have a line of 12 sense wires alternating with shaper wires every 3.8 mm, running down the middle of two gold-on-mylar cathode planes which are separated by ~ 2 cm. Four axial and four stereo superlayers will provide 96 measurements between 44 and 132 cm, requiring a total of 2,520 drift cells and 30,240 readout channels. The wires and cathode planes are strung between two precision milled endplates, and the complete chamber is roughly 1.3% of a radiation length at normal incidence.

The COT is read out using a pipelined TDC which is standard for CDF II wire chamber systems, and the tracking information will be available for the Level-1 trigger.

The COT construction, operation, and off-line reconstruction draw heavily on the experience with the CTC, leading to a profound economy in time, expense, and code development. Scaling from the known CTC performance we expect comparable mo-

COT	
Radial coverage	44 to 132 cm
Number of superlayers	8
Measurements per superlayer	12
Readout coordinates of SLs	+3° 0 -3° 0 +3° 0 -3 0°
Maximum drift distance	0.88 cm
Resolution per measurement	180 μ m
Rapidity coverage	$ \eta \leq 1.0$
Number of channels	30,240
Material thickness	1.3% X_0

SVX II	
Radial coverage	2.4 to 10.7 cm, staggered quadrants
Number of layers	5
Readout coordinates	r- ϕ on one side of all layers
Stereo side	r-z, r-z, r-uv, r-z, r-uv (uv \equiv 1.2° stereo)
Readout pitch	60-65 μ m r- ϕ ; 60-150 μ m stereo
Resolution per measurement	12 μ m (axial)
Total length	96.0 cm
Rapidity coverage	$ \eta \leq 2.0$
Number of channels	405,504
Material thickness	3.5% X_0
Power dissipated	1.8 KW

ISL	
Radial coverage	20 to 28 cm
Number of layers	one for $ \eta < 1$; two for $1 < \eta < 2$
Readout coordinates	r- ϕ and r-uv (1.2° stereo) (all layers)
Readout pitch	110 μ m (axial); 146 μ m (stereo)
Resolution per measurement	16 μ m (axial)
Total length	174 cm
Rapidity coverage	$ \eta \leq 1.9$
Number of channels	268,800
Material thickness	2% X_0

Table 1.1: Design parameters of the baseline tracking systems

CDF Tracking Volume

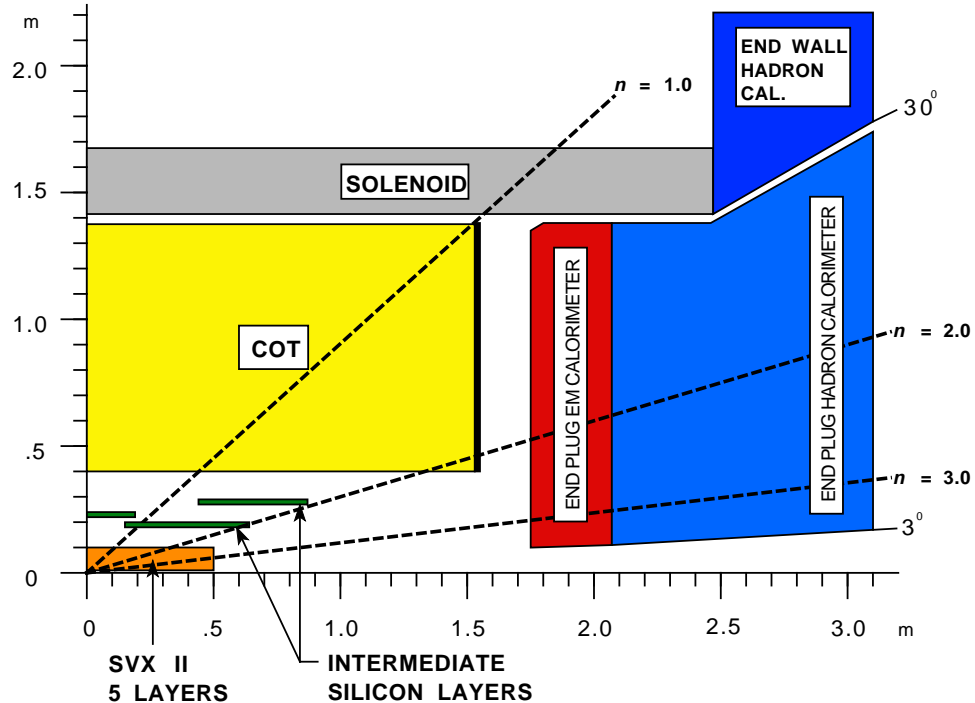


Figure 1.3: Longitudinal View of the CDF II Tracking System

momentum resolution (with SVX II or beam constraint), improved track pair separation, and much improved stereo pattern recognition up to luminosities of $2 \times 10^{32} cm^{-2} s^{-1}$ @ 132 ns. A detailed description of the COT is given in Chapter 4.

1.4.1.2 Inner Tracker: SVX II + ISL

CDF has established the viability and utility of silicon tracking at hadron colliders. For Run II, we propose a silicon “inner tracker” comprising a five-layer detector at small radii for micro-vertex detection and additional silicon layers at intermediate radii to provide stand-alone segment finding in the combined system. As discussed in Chapter 7, stand-alone silicon segments allow integrated tracking strategies which maximize tracking performance over the whole region $|\eta| \leq 2.0$.

SVX II: Silicon Vertex Detector

The silicon vertex detector will be built in three cylindrical barrels with a total length of 96 cm, covering $\sim 2.5\sigma$ of the luminous region, and leading to contained b-tagging in almost all events. Each barrel supports five layers of double sided silicon microstrip detectors between radii of 2.4 and 10.7 cm. Three of

the layers combine an $r - \phi$ measurement on one side with 90° stereo measurement on the other, and the remaining two layers combine $r - \phi$ with small angle stereo at 1.2° .

The silicon crystals are supported by low mass substrates in assemblies called “ladders”. Twelve ladders of the appropriate width make a layer, and the 60 ladders in each barrel are mounted between two precision-machined beryllium bulkheads which also carry the water cooling channels for the readout electronics.

The total of 405,504 channels in the system are connected to radiation-hardened readout chips mounted on electrical hybrids on the surface of the silicon detectors. Each readout chip set (SVX3) has 128 channels, each with a charge-sensitive amplifier, 42-cell dual-ported pipeline with four additional cells for buffers, and an ADC. A highly parallel fiber-based data acquisition system reads out the entire detector in approximately $10 \mu s$.

The high speed and dual porting of the readout allows the SVX II information to be used for impact parameter discrimination in the SVT processor of the Level-2 trigger. The ability to *trigger on b's* adds to the power and generality of the CDF II events, ex-

tends the sensitivity to new phenomena, broadens the catalog of heavy flavor measurements, and provides important control samples for top measurements.

The radiation level at the inner layer is expected to be ~ 0.5 MRad per fb^{-1} . The silicon sensors are expected to operate through inversion, up to a total dose of 1.0-1.5 MRad. A precision locking pin on the bulkheads allows the inner two layers to be removed and replaced with 3 μm accuracy.

ISL: Intermediate Silicon Layers

In the central region, a single ISL layer is placed at a radius of 22 cm. In the plug region, $1.0 \leq |\eta| \leq 2.0$, two layers of silicon are placed at radii of 20 cm and 28 cm. The mechanical problems associated with mounting silicon detectors at these radii are different (and less severe) than in the case of the micro-vertex detector, and in this sense it is logical to treat the ISL as a separate device. We emphasize however, that SVX II and ISL together are a single functional system which provides stand-alone silicon tracking and b-tagging over the full region $|\eta| \leq 2.0$.

Double sided silicon is used with 55 μm strip pitch on the axial side and 73 μm pitch on the stereo side with a 1.2° stereo angle. Every other strip is read out to reduce the total channel count to 268,800. Due to charge sharing through the intermediate strips, the single hit resolution perpendicular to the strip direction will be $\leq 16 \mu\text{m}$ on the axial side and $\leq 23 \mu\text{m}$ on the stereo side.

The silicon crystals are mounted in “ladder” assemblies similar to SVX II. The low radiation levels encountered at larger radii allow the use of longer strips to reduce the channel count. Three crystals are used in each ladder compared to two in SVX II. The ladders are mounted between carbon fiber disks

The ISL readout electronics are identical to the SVX II. The readout segmentation is in 30° wedges which exactly match the SVX II segmentation. This preserves the possibility of adding information from the ISL into the SVT trigger in the future.

1.4.2 Calorimeter Systems

Outside the solenoid, scintillator-based calorimetry covers the region $|\eta| \leq 3.0$ with separate electromagnetic and hadronic measurements. The CDF calorimeters have obviously played a key role in the physics program by measuring electron and photon energies, jet energies, and net transverse energy flow.

$ \eta $ Range	$\Delta\phi$	$\Delta\eta$
0. - 1.1 (1.2 h)	15°	~ 0.1
1.1 (1.2 h) - 1.8	7.5°	~ 0.1
1.8 - 2.1	7.5°	~ 0.16
2.1 - 3.64	15°	0.2 - 0.6

Table 1.2: CDF II Calorimeter Segmentation

	Central	Plug
EM:		
Thickness	$19X_0, 1\lambda$	$21X_0, 1\lambda$
Sample (Pb)	$0.6X_0$	$0.8X_0$
Sample (scint.)	5 mm sheet	4.5 mm fiber
WLS		
Light yield	160 pe/GeV	300 pe/GeV
Sampling res.	$11.6\%/\sqrt{E_T}$	$14\%/\sqrt{E}$
Stoch. res.	$14\%/\sqrt{E_T}$	$16\%/\sqrt{E}$
SM size (cm)	$1.4\phi \times (1.6\text{-}2.0)Z$	$0.5 \times 0.5 \text{ UV}$
Pre-shower size	$1.4\phi \times 65Z \text{ cm}$	by tower
Hadron:		
Thickness	4.5 λ	7λ
Sample (Fe)	1 in. C, 2 in. W	2 in.
Sample (scint.)	10 mm finger	6 mm fiber
WLS		
Light yield	$\sim 40 \text{ pe}/\text{GeV}$	39 pe/GeV

Table 1.3: Central and Plug Upgraded Calorimeter Comparison

As outlined in Sec 1.4.1, the ability to match tracks with projective towers and EM shower position in the central region has lead to a powerful analysis and calibration framework, including an understanding of the absolute jet energy scale to 2.5%.

For Run II, the existing scintillator-based central calorimeters will continue to perform well. However, the gas calorimeters in the region $\eta \geq 1.0$ are incompatible with the crossing rates for Run II, and will be replaced with a new scintillating tile plug calorimeter. As seen in Fig 1.4, the new calorimeter consists of an electromagnetic (EM) section followed by a hadronic section. In both sections the active elements are scintillator tiles read out by wavelength shifting (WLS) fibers embedded in the scintillator. The WLS fibers are spliced to clear fibers, which carry the light out to photomultiplier tubes (PMT) located on the back

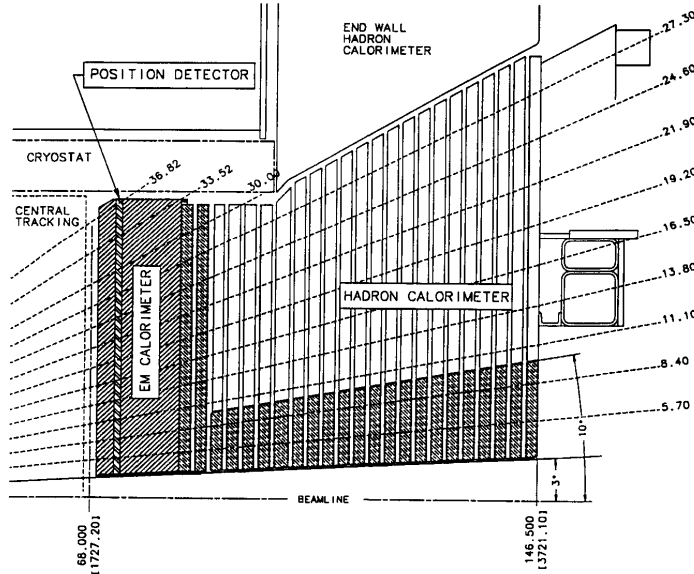


Figure 1.4: Cross section of upper part of new end plug calorimeter.

plane of each endplug.

The EM calorimeter is a lead/scintillator sampling device with a unit layer composed of 4.5 mm lead and 4 mm scintillator. There are 23 layers in depth for a total thickness of about $21 X_0$ (radiation lengths) at normal incidence. The detecting elements are arranged in a tower geometry pointing back towards the interaction region. The energy resolution of the EM section is approximately $16\%/\sqrt{E}$ with a 1% constant term. The scintillator tiles of the first layer of the EM section are made out of 10 mm thick scintillator and are read out by multi-anode photomultipliers (MAPMTs). They will act as a pre-shower detector. A position detector is located at the depth of the EM shower maximum (approximately $6X_0$). This shower maximum detector is made of scintillator strips read out by WLS fibers; clear fibers carry the light to MAPMTs.

The hadron calorimeter is a 23 layer iron and scintillator sampling device with a unit layer composed of 2 inch iron and 6 mm scintillator. The existing iron of the CDF endplugs is used in the new hadron calorimeter: stainless steel disks are attached to the inner 10° cone to extend the coverage to 3° . Two additional stainless steel disks are added behind the electromagnetic section to increase the thickness of the hadron calorimeter. In this way the magnetic field in the tracking volume and the magnetic forces on the end plugs are unchanged. The hadron section

has the same tower segmentation as the EM section.

With the completion of the upgrade, the CDF II calorimeters will have a uniform pattern of matched projective towers of EM and hadron calorimeters. The overall segmentation is given in Table 1.2. The common segmentation pattern continues to allow straightforward calorimetry trigger implementation. Both EM calorimeters have stereo shower maximum detectors as well as pre-shower capability. The EM sections are all lead scintillator sampling and the hadronic sections are iron scintillator sampling.

The central and plug upgrade calorimeters both have fast enough energy measurement response times to take full advantage of the 132 ns bunch spacing. Shower maximum and pre-shower functions in the plug upgrade are also fast enough, while the wire chamber pre-shower and shower maximum in the central system will need to integrate several bunches. A general comparison of the central and plug upgrade calorimeters is given in Table 1.3.

1.4.3 Muon Systems

CDF II will use four systems of scintillators and proportional chambers in the detection of muons over the region $|\eta| \leq 2.0$. The absorbers for these systems are the calorimeter steel, the magnet return yoke, additional steel walls, and the steel from the Run I forward muon toroids. The geometric and engineer-

	CMU	CMP/CSP	CMX/CSX	IMU
Pseudo-rapidity coverage	$ \eta \leq \sim 0.6$	$ \eta \leq \sim 0.6$	$\sim 0.6 \leq \eta \leq \sim 1.0$	$\sim 1.0 \leq \eta \leq \sim 1.5$
Drift tube cross-section	2.68 x 6.35 cm	2.5 x 15 cm	2.5 x 15 cm	2.5 x 8.4 cm
Drift tube length	226 cm	640 cm	180 cm	363 cm
Max drift time	800 ns	1.4 μ s	1.4 μ s	800 ns
Total drift tubes (present)	2304	864	1536	none
Total drift tubes (Run II)	2304	1076	2208	1728
Scintillation counter thickness		2.5 cm	1.5 cm	2.5 cm
Scintillation counter width		30 cm	30-40 cm	17 cm
Scintillation counter length		320 cm	180 cm	180 cm
Total counters (present)		128	256	none
Total counters (Run II)		269	324	864
Pion interaction lengths	5.5	7.8	6.2	6.2-20
Minimum detectable muon p_T	1.4 GeV/c	2.2 GeV/c	1.4 GeV/c	1.4-2.0 GeV/c
Multiple scattering resolution	12 cm/ p (GeV/p)	15 cm/ p	13 cm/ p	13-25 cm/ p

Table 1.4: Design Parameters of the CDF II Muon Detectors. Pion interaction lengths and multiple scattering are computed at a reference angle of $\theta = 90^\circ$ in CMU and CMP/CSP, at an angle of $\theta = 55^\circ$ in CMX/CSX, and show the range of values for the IMU.

ing problems of covering the full η region using these absorbers leads to the four logical systems, but as seen in Table 1.4, they are all functionally similar.

The central muon systems functioned well in Run I, and changes for Run II represent incremental improvements. New chambers will be added to the CMP and CMX systems to close gaps in the azimuthal coverage. Each of these additions presents interesting mechanical problems discussed in detail in Chapter 10. In the CMU system, the cell gang-ing scheme will be changed from alternate cells to adjacent cells, improving the granularity at the trigger level from a 5° azimuthal arc to 2.5° . In addition, because of the high rates in Run II, the CMU chambers will be run in proportional, rather than limited streamer mode, and this requires that gain be recovered by installing new pre-amplifiers on the chambers. In the CMP system, new pre-amps will eliminate intermittent problems with oscillations. In all of these systems, the long drift times relative to the beam crossing time necessitate a pipelined TDC, which is described in detail in Secs. 11.3 and 11.4.

Detailed studies of occupancy and aging for these systems have been performed using the the Run I data set. Extrapolating these results to Run II conditions, including the absence of the Main Ring, and beam pipe shielding, we expect that these systems will show *improved* performance in Run II. Further

detail can be found in Chapter 10.

The CDF II tracking system, particular the ISL, provides a new capability for muon detection, the ability to reconstruct trajectories with $|\eta| > 1.0$ in the solenoid, where the resolution is not dominated by multiple scattering. The region contiguous with the present coverage, $1.0 \leq |\eta|$ and extending out to $|\eta| \sim 2.0$ is most important for improved acceptance for the decays of heavy centrally produced objects. The Run I forward muon system, even if pushed up, would cover only $|\eta| \geq 1.5$, and worse, has low granularity which translates into high occupancy and uncertain efficiency at the high luminosities of Run II.

These considerations motivate the replacement of the forward muon system with a new Intermediate Muon System (IMU), covering from $1.0 \leq |\eta| \leq 1.5$ with fine granularity, and providing coverage sufficient to identify isolated high p_T tracks as muons or hadrons between $\eta = 1.5$ and $\eta = 2.0$. The IMU consists of a barrel of drift chambers and scintillation counters around the present FMU toroid steel, with additional counters between the toroids and on the endwall to provide additional projectivity at the trigger level. The IMU chambers and counters are virtually identical to the existing central muon detectors and use the same readout electronics. The toroids will not be energized; the p_T measurement will be provided by the tracking systems. The IMU system

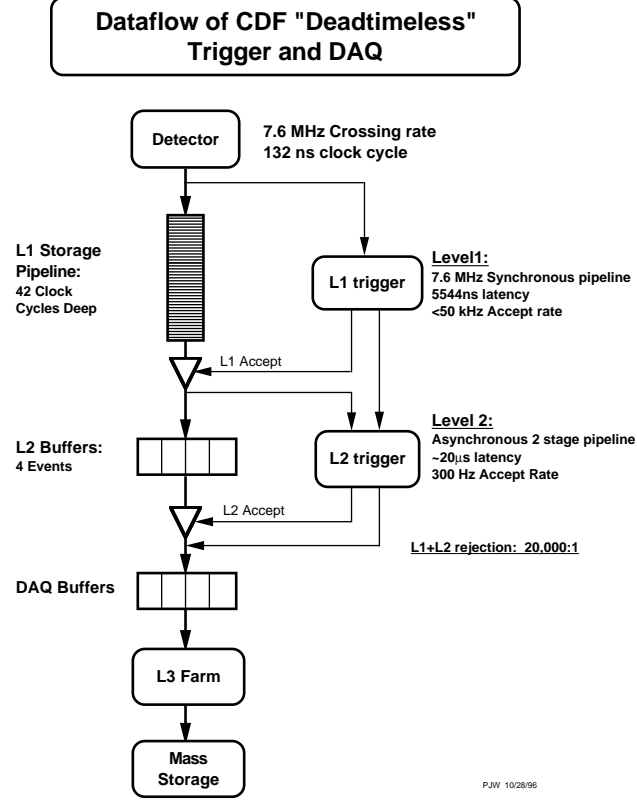


Figure 1.5: Functional block diagram of the CDF II data flow

covers more solid angle and in the more crucial region of lower η than the FMU, will have improved momentum resolution and corresponding trigger improvements, and will operate at luminosities substantially greater than expected during Run II. Further detail on this system can be found in Sec. 10.6.

1.4.4 Electronics and Triggering

The CDF electronics systems must be substantially altered to handle Run II accelerator conditions. The increased instantaneous luminosity requires a similar increase in data transfer rates. However it is the reduced separation between accelerator bunches that has the greatest impact, necessitating a new architecture for the readout system.

Figure 1.5 shows the functional block diagram of the readout electronics. To accommodate a 132 ns bunch-crossing time and a 4 μ s decision time for the first trigger level, all front-end electronics are fully pipelined, with on-board buffering for 42 beam crossings. Data from the calorimeters, the central track-

ing chamber, and the muon detectors are sent to the Level-1 trigger system, which determines whether a $\bar{p}p$ collision is sufficiently interesting to hold the data for the Level-2 trigger hardware. The Level-1 trigger is a synchronous system with a decision reaching each front-end card at the end of the 42-crossing pipeline. Upon a Level-1 trigger accept, the data on each front-end card are transferred to one of four local Level-2 buffers. The second trigger level is an asynchronous system with an average decision time of 20 μ s.

A Level-2 trigger accept flags an event for read-out. Data are collected in DAQ buffers and then transferred via a network switch to a Level-3 CPU node, where the complete event is assembled, analyzed, and, if accepted, written out to permanent storage. These events can also be viewed by online monitoring programs running on other workstations.

1.4.4.1 Front-End Electronics

The installation of new scintillator-based calorimeters in the plug region allows a common design to be used for much of the front-end electronics for the central and plug calorimeters and their associated preradiators and shower-maximum detectors. The calorimeter ADC readout is based on the QIE (Charge Integrating and Encoding) chip, a custom multi-ranging circuit developed for the KTEV experiment. A VME based front-end board carries the QIE, a commercial ADC, and programmable circuits to perform pipelining, buffering, and the creation of traverse-energy sums for the trigger. A simplified version of the QIE design is used for all shower maximum and pre-shower detectors.

Dynode signals from the phototubes for the central, wall, and plug hadron calorimeters will be discriminated and timed using the custom pipelined TDC chip described below.

Analog drift time signals from the COT are first processed using a custom chip, ASD, optimized for the straw systems in the SDC and ATLAS detectors. The eight channel chip has a fast, low noise preamplifier, ion tail cancellation, and a discriminator. The ASD's are mounted on printed circuit boards on the chamber endplate. The discriminated signals are read out with a custom multi-hit TDC, JMC96, which encodes leading and trailing edge information, and has the 5.3 microsecond Level-1 buffer and four Level-2 buffers on-chip. The design includes a full custom integrated circuit, 96 channel VME

boards, and a calibration system.

As described above in Sec. 1.4.3, we are building new preamps and ASD's for the central muon system, CMU, and changing the mother-board system (but not the pre-amplifier) for the CMP muon system. Drift time information from all muon systems will be recorded using the JMC96 TDC.

1.4.4.2 Data Acquisition

A block diagram of the data acquisition system is shown in Fig. 1.6. The basic architecture is very similar to that used successfully in Run Ib. Front-end and trigger electronics are housed in VME crates replacing the FASTBUS and RABBIT crates used in the original detector. Timing signals associated with the beam crossing are distributed to each crate by the Master-Clock subsystem. Trigger decision information is distributed by the Trigger-System-Interface subsystem. Commercial processors read data from modules in their local crate and deliver it to the VME Readout Boards (VRBs) and the Event-Building subsystem. This system concentrates the data and delivers it to the Level-3 trigger subsystem through a commercial network switch. The Level-3 trigger is a “farm” of parallel processors, each fully analyzing a single event. The Data-Logging subsystem delivers events to mass storage and also to online monitoring processes to verify that the detector, trigger, and data acquisition system are functioning correctly. While the architecture is similar to the Run Ib system, many individual components will be upgraded or replaced. This is necessary to deal with the new VME-based front-end electronics, and to provide increased throughput required for the higher luminosity now expected in Run II. Also, in some cases commercial products in the Run Ib system are no longer supported by the manufacturer and must be replaced.

1.4.4.3 Trigger

In Run Ib, the trigger had to reduce the raw collision rate by a factor of 10^5 to reach < 10 Hz, an event rate that could be written to magnetic tape. With an order of magnitude increase in luminosity for Run II, the trigger must have a larger rejection factor while maintaining high efficiency for the broad range of physics topics we study.

We will use a tiered “deadtimeless” trigger architecture. The event is considered sequentially at three

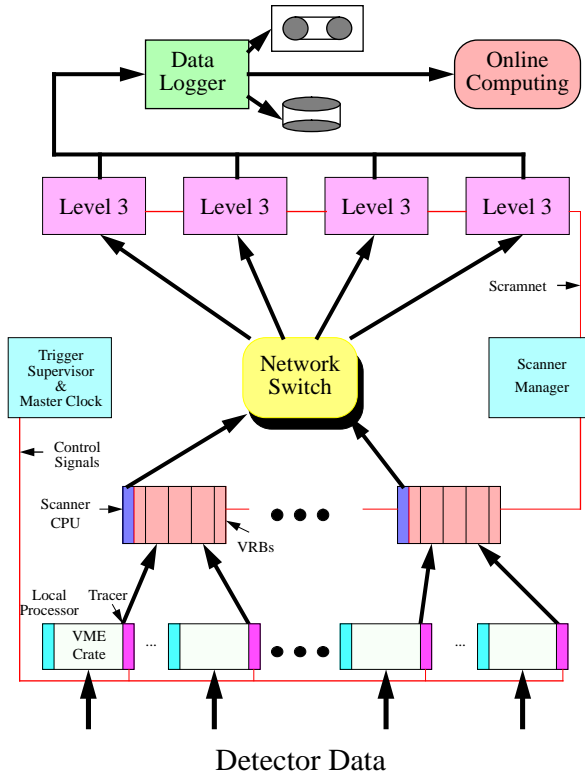


Figure 1.6: A schematic of the CDF II Data Acquisition system, showing data flow from the front-end and trigger VME crates to the Online Computing system.

levels of approximation, with each level providing sufficient rate reduction for the next level to have minimal deadtime. Level-1 and Level-2 use custom hardware on a limited subset of the data and Level-3 uses a processor farm running on the full event readout. The trigger, like the DAQ, is fully pipelined, and has improved background rejection over Run I from additional detector information to be supplied to the Level-1 and Level-2 systems.

The block diagram for the CDF II trigger system is presented in Fig. 1.7. The most significant change for Level-1 is the addition of track finding, which was previously available only at Level-2. This allows a track to be matched to an electromagnetic calorimeter energy cluster for improved electron identification, or to a stub in the muon system for better muon identification and momentum resolution. Also, tracks may be used alone for triggers such as $B^0 \rightarrow \pi^+ \pi^-$. A Level-1 accept can also be generated based on calorimeter energy, E_T , or the kinematic properties of observed track pairs.

Events accepted by the Level-1 system are pro-

RUN II TRIGGER SYSTEM

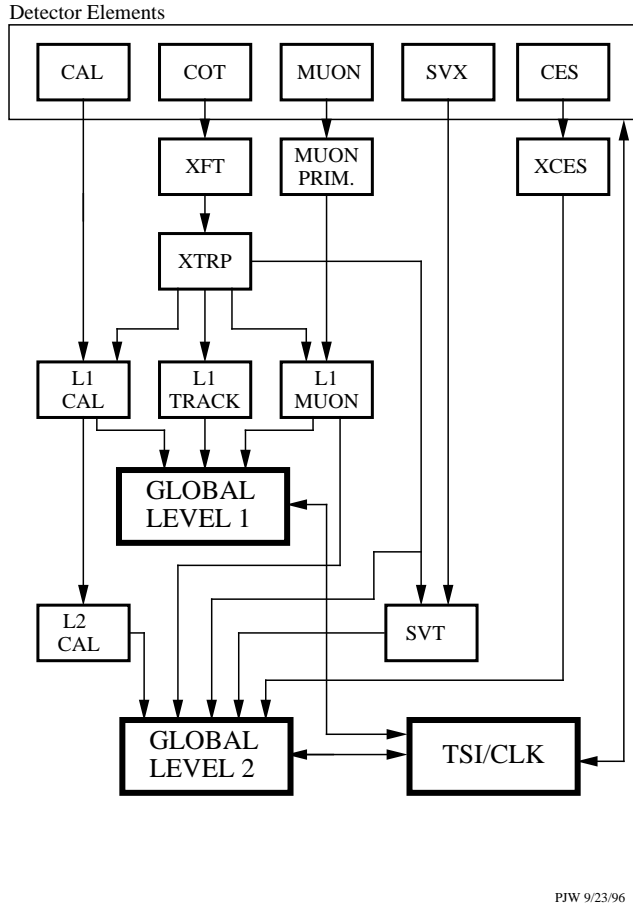


Figure 1.7: Block diagram of the CDF II trigger system.

cessed by the Level-2 hardware, which will also have more and improved input data. The Silicon Vertex Tracker (SVT) will provide, for the first time in a hadron-collider experiment, the ability to trigger on tracks with large impact parameters. This will make accessible a large number of important processes involving hadronic decay of b -quarks, such as $Z \rightarrow b\bar{b}$, $B^0 \rightarrow \pi^+\pi^-$, and exotic processes like SUSY and Technicolor that copiously produce b quarks. The Level-2 system will have improved momentum resolution for tracks, finer angular matching between muon stubs and central tracks, and data from the central shower-max detector (CES) for improved identification of electrons and photons. Jet reconstruction is provided by the Level-2 cluster finder, which, although rebuilt for the new architecture, retains the same algorithm used successfully in previous running.

The trigger system is very flexible and will be able

to accommodate over 100 separate trigger selections. With a 40 kHz accept rate at Level-1 and a 300 Hz rate out of Level-2, we expect to limit deadtime to $< 10\%$ at full luminosity, while writing events to mass storage at 30-50 Hz. Rates for the more challenging signatures are discussed at the end of Chapter 12.

1.5 The CDF II Upgrade Plan

Our goal is to rebuild CDF into CDF II as quickly as possible, and resume data taking at the Tevatron in a timely way after the completion of the Main Injector.

Because of the realities of budget and schedule, our proposal for CDF II accepts some compromises to the goals outlined in Sec. 1.3.2. In particular, we will defer further discussion of the time-of-flight system and full trigger capability at $|\eta| \geq 1.0$ until the baseline detector described in this document is convincingly in hand.

This document is the TECHNICAL DESCRIPTION of the baseline CDF II detector. Additional documents describe the managerial, cost, and schedule aspects of the project:

- CDF Project Management Plan
- Memoranda of Understanding (MOU) and Work Plans for each subproject
- Cost and Schedule Plan
 - Task-based resource-loaded schedule, including labor estimates
 - Cost Estimate and Work Breakdown Structure (WBS), including contingency analysis
 - WBS Dictionary
 - Financial Plan for U.S. and non-U.S. funding

1.5.1 Outlook

The baseline scope of the detector proposed here meets every goal for a rejuvenated detector capable of operations with the Tevatron + Main Injector at $\mathcal{L} = 2 \times 10^{32} \text{ cm}^{-2}\text{s}^{-1}$ and 132 ns bunch spacings.

- The tracking system will be a fully optimized combination of drift chamber and silicon with powerful redundancy that insures excellent pattern recognition, momentum resolution, and b-tagging out to $|\eta| = 2$, even in the presence of multiple interactions.

- The calorimetry will be exclusively scintillator based, fast, and have resolution equal to or better than the existing detector.
- The muon system will have almost full azimuthal coverage in the central region, and expanded coverage out to $|\eta| = 2.0$.
- The electronics will be fully compliant with the 132 ns bunch crossing in every channel, and the data acquisition system and Level-3 trigger will be capable of 300 Hz operation.
- The trigger will be deadtimeless, ready for every crossing, with tracking information at Level-1 and impact parameter discrimination at Level-2.

This design reflects the accumulated experience of a decade of physics with CDF at the Tevatron. With CDF II and anticipated data sets in excess of 2 fb^{-1} in Run II, we look forward to major discoveries at Fermilab in the decade to come.